ELSEVIER

Engineering Analysis with Boundary Elements 31 (2007) 200–208

ENGINEERING ANALYSIS with BOUNDARY ELEMENTS

www.elsevier.com/locate/enganabound

DRM-MD approach for modeling laser–material interaction with axial symmetry

Radovan Gospavić[a], Viktor Popov[a,*], Milesa Srecković[b], C.S. Chen[c]

[a]*Wessex Institute of Technology, Ashust Lodge, Southampton, UK*
[b]*Faculty of Electrical Engineering, Bulevar Kralja Aleksandra 73, Belgrade, Serbia and Montenegro*
[c]*University of Southern Mississippi, USA*

Received 30 May 2006; accepted 14 September 2006
Available online 15 November 2006

Abstract

A dual reciprocity method multi-domain (DRM-MD) approach for modeling laser–material interaction with axial symmetry was developed. The proposed approach is based on the fundamental solution for the Laplace equation in 2D and is much simpler for implementation than the dual reciprocity boundary element method (DRBEM) based on the fundamental solution for axisymmetric problems incorporating elliptic integrals. The thermal model of laser–material interaction was applied for the cases of mono as well as multi-layer structures. Different aspects of interaction up to the melting point of considered materials are presented. The effect of temperature dependence of the absorption coefficients on the process of laser heating was considered. Numerical results for spatial as well as temporal temperature distribution inside the material bulk are presented and compared to analytical solutions.

Keywords: Laser–material interaction; Axisymmetric problem; Boundary element method; Dual reciprocity method multi-domain approach

1. Introduction

The dual reciprocity method multi-domain (DRM-MD) approach was applied for laser–material interaction analysis. Laser beams have a number of applications in different areas of science, technology, material machining, medicine [1–3], etc. In the present work, time-dependent thermal models of interaction in case of cylindrical geometry and mono as well as multi-layer structures were considered. The numerical model of laser–material interaction described here is restricted only to heating effects of the targeted material without destructive and disintegration processes during interaction, i.e. the incident intensity of laser radiation was considered to be less or equal to critical intensity. Although some analytical solutions of thermal interaction exist, they are mainly for one- or two-dimensional cases (2D) [4,5]. Use of numerical approaches offers the possibility of analyzing more complicated cases which are of interest in real-world applications. The numerical methods allow for various boundary and initial conditions, geometry, as well as temporal and spatial distributions of loads, to be used.

The dual reciprocity method (DRM) was introduced by Nardini and Brebbia [6], and is based on the boundary element method (BEM) which transforms the governing partial differential equation (PDE) using Green's second identity into an equivalent integral equation over the boundary of the considered domain. The BEM requires the fundamental solution for the governing PDE to be available in closed form [7], otherwise, the additional terms of the PDE, that are not considered when the fundamental solution is derived, would appear in a domain integral. To avoid this kind of problems the DRM was introduced, which transforms the domain integral into an integral over the boundary, preserving this way the boundary nature of the numerical scheme. The starting boundary integral equation is further transformed into equivalent system of linear equations by meshing the boundary of the problem domain, expressing unknown functions using their nodal

*Corresponding author. Tel.: +44 2380 293 223; fax: +44 2380 292 853.
E-mail addresses: gospavic@wessex.ac.uk (R. Gospavić), viktor@wessex.ac.uk (V. Popov), sreckovic@tesla.rcub.bg.ac.yu (M. Srecković), cschen.math@gmail.com (C.S. Chen).

0955-7997/$ - see front matter © 2006 Elsevier Ltd. All rights reserved.
doi:10.1016/j.enganabound.2006.09.006

values and interpolation function, evaluating the boundary integrals over each boundary element and applying the given boundary conditions.

The advantages of these approach in engineering applications and various numerical analysis relative to domain methods, such as the finite element method (FEM) [8], is in the fact that only the boundary of the problem domain needs to be discretized, saving this way efforts in model preparation. However, for large problems the domain methods have lower CPU and memory requirements than the BEM.

The dual reciprocity method-multi-domain (DRM-MD) approach was introduced by Popov and Power [9] who noticed that the DRM formulation combined with domain decomposition leads to substantial improvement in accuracy and convergence of the DRM. The formulation was initially applied to the problem of flow of mixture of gases through a porous media [10,11]. Further applications included solution of the Navier–Stokes equation [12], non-Newtonian flow problems at low Reynolds number [13] and flow and solute transport in fractured porous media [14,15].

The DRM-MD is based on decomposition of the problem domain into sub-regions and applying DRM approach on each of the sub-regions separately with corresponding matching conditions on the interface of the adjacent sub-domains. The main advantage of the DRM-MD is that the size of the sub-domains can be adjusted throughout the domain according to what the problem under consideration requests in order that the optimal solution procedure in terms of efficiency and accuracy is achieved. In other words, the DRM-MD is capable of utilizing the advantages of both types of numerical techniques, i.e. domain based and boundary-based techniques.

In the case of axisymmetric problems a major difficulty is finding a suitable particular solution for a given basis function [16–18]. In this work the DRM-MD approach was implemented for axisymmetric problems, where the Laplace operator in cylindrical coordinates was divided into two parts: a corresponding Laplace operator in a rectangular coordinate system and a term arising due to the cylindrical coordinate system. The fundamental solution for the Laplace equation in 2D was applied and the term due to the cylindrical coordinate system was considered to be additional term in the non-homogeneous part of the Laplace equation, which was accounted for through the DRM approximation.

The limiting value for the axial part of the Laplace operator on the z-axis was evaluated by taking into account the physical processes of the analyzed problem, and should be considered for each problem separately. For the problem of heat transfer the limiting value was evaluated according to the physical low for conservation of thermal energy.

2. Mathematical model of interaction

The heating process provoked by a laser beam during interaction was assumed to be due to absorption of the laser beam in the thin surface layer of the bulk material. The interaction with the material was modeled as an equivalent surface thermal source with appropriate spatial and temporal distributions. This work was focused on cylindrical specimens and surface distributions of absorbed incoming laser beam fluxes, and accordingly the temperature field analysis was performed using the cylindrical coordinate system. Though this problem is a three-dimensional one, as axial symmetry exists, the temperature field is a function of the radial and axial coordinates only, i.e. the problem under consideration becomes a 2D one. In this work only mono and two layer structures, with ideal thermal contacts between adjacent layers, were considered. Nevertheless, the results can be applied to multi-layer structures and imperfect/perfect thermal contact as well as well. The geometry of the considered problem for a two-layer case is shown in Fig. 1.

It was assumed that the spatial and temporal distributions of the laser beam intensity on the surface of the material specimens could be described by a product of two independent functions of the radial coordinate and time, e.g. $q(r)$ and $\varphi(t)$, respectively [4].

It was assumed that all the thermal parameters of the material of interest in the considered temperature range are constant and temperature independent, while the absorption coefficient was considered to depend on the temperature in a linear fashion [4]. The initial temperature inside the specimen was supposed to be equal to the ambient temperature T_0. Heating of the specimen, according to the above assumptions, for a two layer cylindrical structure (Fig. 1.), with ideal thermal contact between layers, could be described by the following equations [4]:

$$\frac{1}{a_1}\frac{\partial T_1(z,r,t)}{\partial t} = \Delta T_1(z,r,t);\ 0\leqslant z\leqslant h_1;\ t\geqslant 0;\ 0\leqslant r\leqslant R,$$
$$\frac{1}{a_2}\frac{\partial T_2(z,r,t)}{\partial t} = \Delta T_2(z,r,t);\ h_1\leqslant z\leqslant h;\ t\geqslant 0;\ 0\leqslant r\leqslant R. \quad (1)$$

Subscripts 1 and 2 correspond to the upper and to the lower layer, respectively. The corresponding boundary

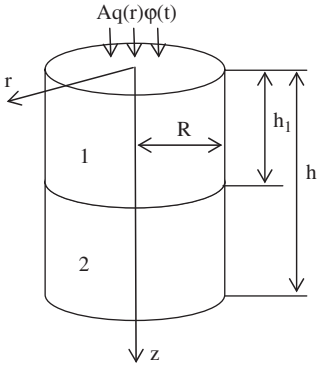

Fig. 1. Geometry of the problem domain (R—radius of the structure; h_1—thickness of upper layer; h—height of whole structure; A—absorption coefficient).

conditions are:

$$-\lambda_1\frac{\partial T_1}{\partial z}=A(T)q(r)\varphi(t),\ z=0,\ 0\leqslant r\leqslant R;$$
$$-\lambda_1\frac{\partial T_1}{\partial r}=\alpha_1 T_1,\ r=R,\ 0\leqslant z\leqslant h_1,$$
$$-\lambda_2\frac{\partial T_2}{\partial r}=\alpha_2 T_2,\ r=R,\ h_1\leqslant z\leqslant h;$$
$$-\lambda_2\frac{\partial T_2}{\partial z}=\alpha_2 T_2,\ z=h,\ 0\leqslant r\leqslant R, \tag{2}$$
$$T_1=T_2,\ \lambda_1\frac{\partial T_1}{\partial z}=\lambda_2\frac{\partial T_2}{\partial z};\ z=h_1,\ 0\leqslant r\leqslant R,$$
$$\frac{\partial T_1}{\partial r}=0;\ r=0,\ 0\leqslant z\leqslant h_1;\ \frac{\partial T_2}{\partial r}=0;\ r=0,\ h_1\leqslant z\leqslant h,$$

where T is the temperature difference between the interior domain temperature and ambient one, λ is the coefficient of thermal conductivity, $a=\lambda/\rho\cdot c$ is the coefficient of thermal diffusivity, c is the specific heat, ρ is the material density, α is heat transfer coefficient which determines the rate of thermal losses on boundary surface, R and h are specimen's radius and length, respectively, and $A(T)$ is absorption coefficient of the laser radiation by the material of the upper layer at temperature difference T.

The temperature dependence of the absorption coefficient is assumed to follow the following linear form

$$A(T)=A_0+B\cdot T, \tag{3}$$

where A_0 is of the absorption coefficient at ambient temperature T_0 and B are constants whose value depend on the type of material [4]. For Al the above constants have the following numerical values: $A_0=0.642$; $B=-4.28\times 10^{-4}\frac{1}{K}$.

The thermal losses, in axial and radial directions, were modeled by free thermal convection. Structures with three or more layers could also be described by the above model.

3. The dual reciprocity method (DRM)

If we consider a mono-layer structure, the governing Eq. (1) at nth time step could be transformed in the following form:

$$\frac{\partial^2 T}{\partial r^2}+\frac{\partial^2 T}{\partial z^2}=\frac{1}{a}\frac{\partial T}{\partial t}-\frac{1}{r}\frac{\partial T}{\partial r}=b;\ 0\leqslant r\leqslant R;\ 0\leqslant z\leqslant h,$$
$$b=b_1-b_2;\ b_1=\frac{1}{a}\frac{\partial T}{\partial t}\approx\frac{1}{a\Delta t}(T(r,z,(n+1)\Delta t)-T(r,z,n\Delta t))=\frac{1}{a\Delta t}(T_{n+1}-T_n);\ b_2=\frac{1}{r}\frac{\partial T}{\partial r}, \tag{4}$$

where Δt is time step. The fundamental solution for the Laplace equation in 2D is given by [7]:

$$\Delta T^*(|x|)+\delta(x)=0;\ \Delta=\frac{\partial^2}{\partial r^2}+\frac{\partial^2}{\partial z^2};$$
$$|x|=\sqrt{r^2+z^2};\ T^*(|x|)=\frac{1}{2\pi}\ln\left(\frac{1}{|x|}\right);\ x=(r,z). \tag{5}$$

By applying the Green's identity (4) can be transformed into the following integral form [7]:

$$\chi(x)\cdot T(x)+\int_{\Gamma_y}q^*(|x-y|)\cdot u(y)\,\mathrm{d}\Gamma_y-\int_{\Gamma_y}T^*(|x-y|)\cdot q(y)\,\mathrm{d}\Gamma_y=-\int_{\Omega_y}T^*(|x-y|)\cdot b(y)\,\mathrm{d}\Omega_y, \tag{6}$$

$$\chi(x)=\begin{cases}1, & x\in\Omega,\\ \theta/2\pi, & x\in\Gamma;\ \Omega=\{(r,z)|0\leqslant r\leqslant R,0\leqslant z\leqslant h\},\ \Gamma=\partial\Omega,\\ 0, & x\notin\Omega,\end{cases}$$

where θ is the internal angle at boundary point x in radians, $x=(r_x,z_x)$, $y=(r_y,z_y)$, Ω is the problem domain, Γ is the contour that encloses the domain Ω, n is the direction of the normal to Γ, and $q=\partial T/\partial n; q^*=\partial T^*/\partial n$.

To avoid domain integration on the right-hand side in (6) the non-homogenous term b could be expanded using approximation functions in the following form [19]:

$$b(y)\approx\tilde{b}(y)=\sum_{j=1}^{N+L}\alpha_k f(|y-y_j|)+P(y), \tag{7}$$

where α_k are unknown coefficients; $f(|y-y_j|)$ is approximation function, which belongs to a family of conditionally positive definite (CPD) radial basis functions (RBFs) of order k; P is a polynomial of order $k-1$; $|y-y_j|$ is a distance between fixed collocation point y_j and point y where the function is approximated; L and N are the number of boundary and internal nodes, respectively, and $y=(r_y,z_y)$; $y_j=(r_j,z_j)$ [20].

The above equation is identically satisfied in all collocation nodes. The following additional equations are used to achieve uniqueness of the solution of the above system of equations [20]:

$$\sum_{j=1}^{N+L}\alpha_j\cdot r_j^{\beta}=0;\ \sum_{j=1}^{N+L}\alpha_j\cdot z_j^{\beta}=0;\ \beta=0,\ 1,\ldots,\ k-1. \tag{8}$$

Next, an auxiliary function $\hat{u}(y,y_j)$ is introduced in the following way [12]:

$$\Delta\hat{u}(y,y_j)=\frac{\partial^2\hat{u}(y,y_j)}{\partial r_y^2}+\frac{\partial^2\hat{u}(y,y_j)}{\partial z_y^2}=f(|y-y_j|). \tag{9}$$

Instead of using particular solutions for Laplace's operator in cylindrical coordinates, particular solutions for Laplace's operator in rectangular coordinates were used, which can be expressed in analytical form for a large number of RBFs [16]. Accordingly, much easier DRM-MD numerical approach for axisymmetric problems was obtained.

Using expressions (7) and (9) the domain integral in (6) could be transformed in the following way:

$$\begin{aligned}\int_{\Omega_y} b(y)T^*(|x-y|)\,\mathrm{d}\Omega_y &= \sum_{j=1}^{N+L}\alpha_j\int_{\Omega_y}\Delta\hat{u}(y,y_j)T^*(|x-y|)\,\mathrm{d}\Omega_y\\ &= -\sum_{j=1}^{N+L}\alpha_j(\chi(x)\hat{u}(x,y_j)\\ &\quad+\int_{\Gamma_y}\hat{u}(y,y_j)q^*(|x-y|)\\ &\quad-\hat{q}(y,y_j)T^*(|x-y|)\,\mathrm{d}\Gamma_y),\end{aligned}\tag{10}$$

where $\hat{q}(y,y_j)=(\partial\hat{u}(y,y_j))/\partial n_j$.

By substituting (10) into (6) the next equation is obtained [19]:

$$\begin{aligned}&\chi(x)T(x)+\int_{\Gamma_y}(T(y)q^*(|x-y|)-T^*(|x-y|)q(y))\,\mathrm{d}\Gamma_y\\ &\quad=\sum_{j=1}^{N+L}\alpha_j(\chi(x)\hat{u}(x,y_j)+\int_{\Gamma_y}(\hat{u}(x,y_j)q^*(|x-y|)\\ &\quad-\hat{q}(y,y_j)T^*(|x-y|))\,\mathrm{d}\Gamma_y).\end{aligned}\tag{11}$$

The limiting value of the term $1/r\cdot(\partial T/\partial r)$ along z-axis could be determined by using the law for conservation of thermal energy. The thermal flux through the elementary surface S which encloses elementary volume $\mathrm{d}V$ during infinitesimally time period $\mathrm{d}t$, (Fig. 2.), could be expressed through the following relations:

$$\begin{aligned}&\mathrm{d}V\cdot\rho\cdot c\cdot\mathrm{d}T=-\oint_S\vec{q}\cdot\mathrm{d}\vec{s}\cdot\mathrm{d}t;\ \mathrm{d}T=\frac{\partial T}{\partial t}\mathrm{d}t+\vec{v}\,\nabla T,\ (\vec{v}=0);\\ &\mathrm{d}V=\Delta r^2\pi\cdot\mathrm{d}z,\\ &\oint\vec{q}\cdot\mathrm{d}\vec{s}=q_v\cdot2\Delta r\pi\cdot\mathrm{d}z+(q_{z2}-q_{z1})\Delta r^2\pi\\ &\Rightarrow\frac{\rho\cdot c}{2}\frac{\partial T}{\partial t}=-\left(\frac{q_r}{\Delta r}+\frac{1}{2}\frac{q_{z2}-q_{z1}}{dz}\right),\\ &q_r=-\lambda\frac{\partial T}{\partial r};\ q_z=-\lambda\frac{\partial T}{\partial z}\\ &\Rightarrow\lim_{\Delta r\to0}\frac{1}{\Delta r}\frac{\partial T}{\partial r}=\frac{1}{2}\cdot\left(\frac{1}{a}\frac{\partial T}{\partial t}-\frac{\partial^2T}{\partial z^2}\right),\end{aligned}\tag{12}$$

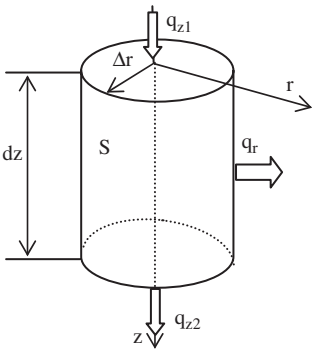

Fig. 2. The thermal flux consideration along z-axis.

where a, ρ and c have same meaning as in relations 1 and 2, $\vec{v}$ is velocity of element $\mathrm{d}V$, $q_{1,2}$ is thermal flux in axial direction at point z and $z+\mathrm{d}z$, respectively, and q_r is thermal flux in radial direction on boundary surface S.

After discretization of the boundary Γ, the unknown functions T and q are interpolated on the linear elements on the boundary [6], the boundary integrals are evaluated and using collocation technique Eq. (11) is transformed into a system of linear equations.

The nodal values $T(x_i)$, $\hat{u}(x_i)$, $q(x_i)$, $\hat{q}(x_i)$, $b(x_i)$, $b_1(x_i)$, $b_2(x_i)$ and the coefficients α_i could be expressed in matrix form as

$$\begin{aligned}&\mathbf{b}=\mathbf{F}\cdot\boldsymbol{\alpha}=[b(y_1)\cdots b(y_K)]_{K\times1},\ \mathbf{F}=[f(y_i,y_j)]_{K\times K},\\ &\boldsymbol{\alpha}=[\alpha_1\cdots\alpha_K]_{K\times1}\Rightarrow\boldsymbol{\alpha}=\mathbf{F}^{-1}\cdot\mathbf{b},\\ &\mathbf{u}=[T(x_1)\cdots T(x_K)]_{K\times1},\ \mathbf{q}=[q(x_1)\cdots q(x_K)]_{K\times1},\\ &\widehat{\mathbf{u}}=[\hat{u}(x_1)\cdots\hat{u}(x_K)]_{K\times1},\ \widehat{\mathbf{q}}=[\hat{q}(x_1)\cdots\hat{q}(x_K)],\end{aligned}\tag{13}$$

$$\mathbf{b}_1=\frac{1}{a\cdot\Delta t}(\mathbf{u}-\mathbf{u}_0);\tag{14}$$

$$b_{2i}=\begin{cases}\sum\limits_{j,n,m}\delta_{ij}\frac{1}{r_i}\frac{\partial f_{jn}}{\partial r}f_{nm}^{-1}T_m,\ r_i\neq0,\\ \frac{1}{2a\Delta t}(T_i-T_{0i})-\sum\limits_{j,n}\frac{1}{2}\frac{\partial^2f_{ij}}{\partial z^2}\cdot f_{in}^{-1}T_n,\ r_i=0,\end{cases}$$

$$\mathbf{b_2}=[b_{21}\cdots b2k]_{K\times1};\ K=N+L,\tag{15}$$

$$\begin{aligned}&\frac{\partial f_{jn}}{\partial r}=\left.\frac{\partial f(y,y_n)}{\partial r}\right|_{y=y_j};\ \frac{\partial^2f_{jn}}{\partial z^2}=\left.\frac{\partial^2f(y,y_n)}{\partial z^2}\right|_{y=y_j},\\ &f_{nm}^{-1}=\left[\mathbf{F}^{-1}\right]_{nm};\ y=(r,z);\ y_n=(r_n,z_n),\end{aligned}\tag{16}$$

where T_{0i} is a temperature obtained in the previous time step at node i, N is the number of boundary nodes, L is the number of internal nodes, $K=N+L$ is the number of all nodes, and δ_{ij} is the Kronecker delta symbol. In the above equations the time derivative was approximated by finite difference.

For some RBFs the second derivative has singularity in collocation nodes and could not be used in above manner. To avoid this problem the second derivative could be expressed in the following way [21]:

$$\begin{aligned}&\mathbf{u}=\mathbf{F}\cdot\boldsymbol{\beta};\ \Rightarrow\frac{\partial\mathbf{u}}{\partial z}=\frac{\partial\mathbf{F}}{\partial z}\cdot\boldsymbol{\beta}=\frac{\partial\mathbf{F}}{\partial z}\cdot\mathbf{F}^{-1}\cdot\mathbf{u},\\ &\frac{\partial\mathbf{u}}{\partial z}=\mathbf{F}\cdot\gamma\Rightarrow\frac{\partial^2\mathbf{u}}{\partial z^2}=\frac{\partial\mathbf{F}}{\partial z}\cdot\gamma=\frac{\partial\mathbf{F}}{\partial z}\cdot F^{-1}\cdot\frac{\partial\mathbf{u}}{\partial z}=\left(\frac{\partial\mathbf{F}}{\partial z}\cdot\mathbf{F}^{-1}\right)^2\cdot\mathbf{u}.\end{aligned}\tag{17}$$

In all the numerical examples presented in this paper, the above expression for second derivatives was used.

Next, (11) could be expressed in matrix form by using the following relations [12]:

$$\mathbf{H}\,\mathbf{u} - \mathbf{G}\,\mathbf{q} = (\mathbf{H}\,\widehat{\mathbf{u}} - \mathbf{G}\,\widehat{\mathbf{q}})\mathbf{F}^{-1}\,\mathbf{b} + \mathbf{I_0}, \tag{18}$$

$$\mathbf{I_0} = [I_{0i}];\ I_{0i} = \frac{A_0}{\lambda}\int_0^{r_0} I(r_y, n\cdot\Delta t)\cdot T^*(|\vec{y} - \vec{y}_i|)\cdot \mathrm{d}r_y,$$
$$\vec{y} = (r_y, 0);\ \vec{y}_i = (r_i, z_i);\ i = 1,\ldots,K, \tag{19}$$

where **H** and **G** are matrices whose matrix elements were evaluated from the contour integrals. The elements of the vector **q** over contour Γ could be expressed, according to the boundary conditions, by the elements of vector **u**. The elements of vector I_0 represent the equivalent thermal loads on upper surface of the specimen.

4. The DRM-MD approach

The DRM-MD approach is based on the decomposition of the problem domain into sub-domains and application of the DRM on each sub-domain separately [19]. At the mth interface between two adjacent sub-domains i and $i+1$, matching conditions are imposed in the following way:

$$T_i|_m = T_{i+1}\big|_m = T|_m;\ \lambda_i\frac{\partial T_i}{\partial n}\bigg|_m = \lambda_{i+1}\frac{\partial T_{i+1}}{\partial n}\bigg|_m, \tag{20}$$

where λ_i and λ_{i+1} are the coefficients of thermal conductivity in the ith and $i+1$th sub-domain, respectively, n is the normal on interface between sub-domains, and $T|_m$ is the temperature on mth interface. In the case of two different layers, as we suppose that thermal contact between layers is ideal, the temperatures in both layers on the interface are equal.

Using the sub-system matrices evaluated from the DRM procedure in each of the sub-domains separately, the system matrix for the DRM-MD formulation is assembled. The DRM-MD system matrix is block-banded matrix with one block for each sub-region and overlaps between the blocks when sub-regions have common interface.

5. Numerical results

5.1. Case study 1

The governing Eq. (1) with corresponding boundary conditions (2) for a single layer homogenous Al specimen using the DRM-MD approach was solved. A specimen of cylindrical geometry (Fig. 1) with the following dimensions: radius $R = 7$ mm and length $h = 5$ mm was considered. Four equal sub-domains of rectangular shape with dimensions 3.5×2.5 mm and with 21 boundary nodes on each side were used. The total number of interior nodes was 268. The following properties of the incoming laser beam were considered: power of incoming laser radiation = 500 W, coefficient of absorption was $A_0 = 0.642$ and $B = 0$, radius of laser beam 1 mm, top head profile and constant laser beam intensity with time duration of 1 s. The following coefficients were used for aluminum: $\lambda_{al} = 240\,\mathrm{W/m\,K}$; $c_{al} = 1021.711\,\mathrm{J/kg}$; $\rho_{al} = 2700\,\mathrm{kg/m^3}$; $a_{al} = \lambda/\rho\cdot c$ and $\alpha_{al} = 10\,\mathrm{W/m^2\,K}$.

The temperature field distribution, in radial and axial direction, with four sub-domains and comparison with analytical solution [22] are presented in Figs. 3 and 4, respectively. The results were obtained by using augmented thin plate spline (ATPS) and the function $1+r$ which was often used in the DRM in the past [19,20]. Both RBF functions produce satisfactory accuracy, with the ATPS being slightly more accurate than $1+r$.

In Figs. 5 and 6 the comparisons of the accuracy are shown along r and z directions, respectively, for the Case study 1, relative to analytical results [22], using ATPS, multi-quadric (MQ) [20] and $1+r$ RBFs. The dimensions of the specimen, the parameters of incident laser beam and

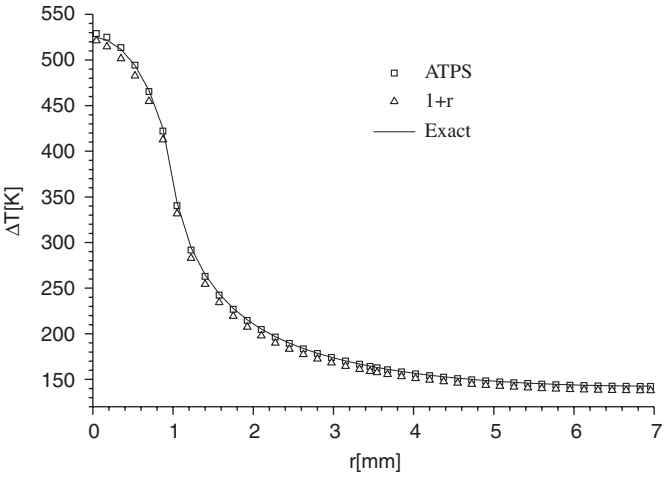

Fig. 3. Distribution of the temperature difference along r-axis, on upper surface of Al specimen obtained using DRM-MD (4 sub-domain), with ATPS and $1+r$ RBFs, compared to analytical solution.

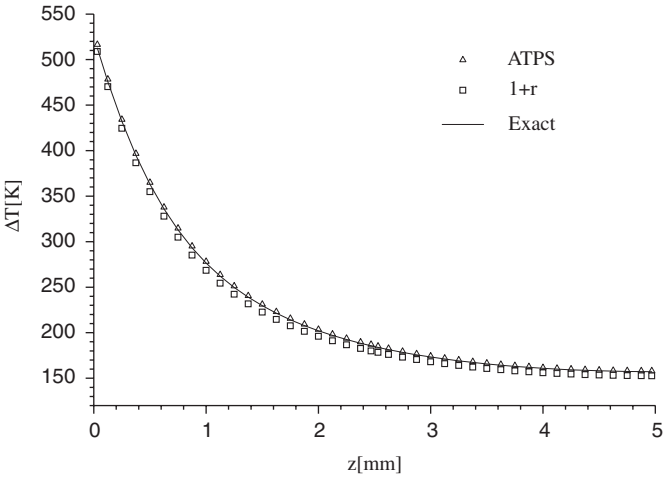

Fig. 4. The distribution of the temperature difference along the z-axis of the Al specimen obtained using DRM-MD (4-sub-domain), with ATPS and $1+r$ RBFs, compared to analytical solutions.

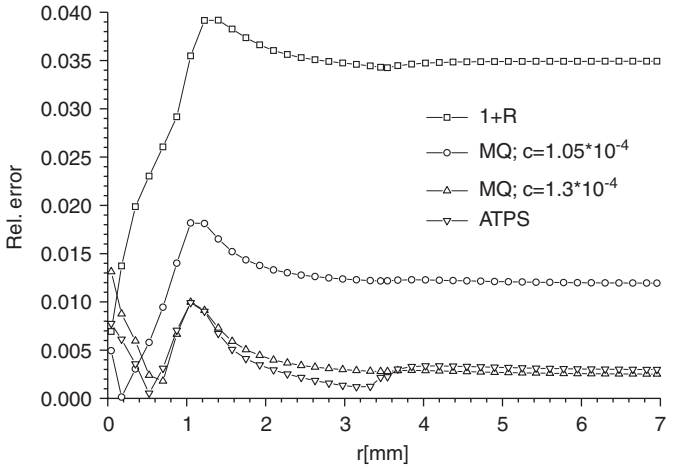

Fig. 5. The relative error for the temperature distribution along r-axis on the upper surface of the Al specimen using ATPS, MQ (for two different values of the shape parameter c), and $1+r$ RBFs.

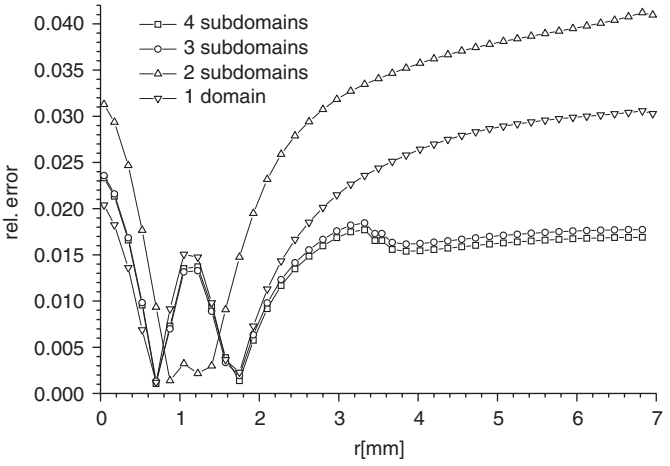

Fig. 7. The relative error for the temperature distribution along r-direction on upper surface of the Al specimen for different number of sub-domains, using the ATPS function.

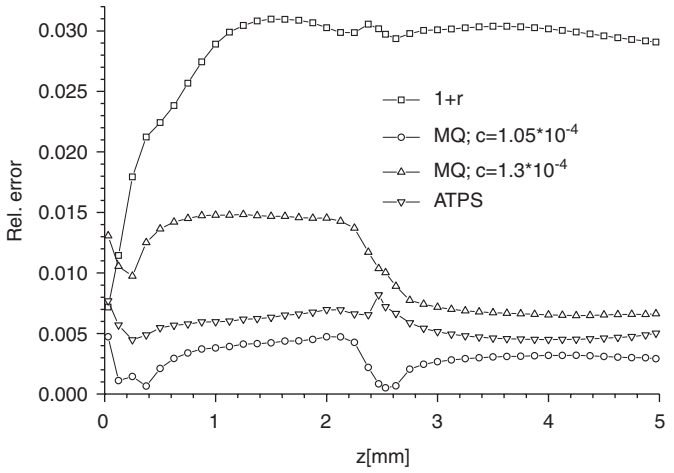

Fig. 6. The relative error for the temperature distribution along z-axis of the Al specimen using ATPS, MQ (for two different value of the shape parameter c), and $1+r$ RBFs.

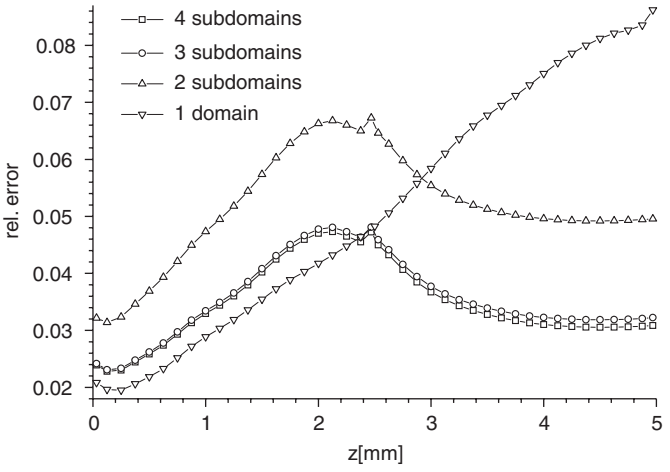

Fig. 8. The relative error for the temperature distribution along z-axis of the Al specimen for different number of sub-domains, using the ATPS function.

the mesh data were the same as in the previous case. Values of shape parameters in a range from 10^{-7} to 10^{3} were tested and the best results were obtained for the value around 10^{-4}. Results for two different values of shape parameter for the MQ function are shown. From Figs. 5 and 6 it could be observed that ATPS and MQ achieved the highest accuracy, though in the case of MQ sensitivity to the value of the shape parameter c was observed. This problem when using MQ RBFs in combination with DRM-MD has already been reported in the open literature [24].

In Figs. 7 and 8 comparison of accuracy for the Case study 1, relative to analytical results, for different number of sub-domains using ATPS-RBFs are presented. The total number and positions of all nodes was fixed, and only the number of subdomains was changed. In the case of subdivision into four sub-domains, four equal rectangular sub-domains with dimensions 3.5×2.5 and 21 boundary nodes on each side were used. The number of interior nodes inside of each sub-domain was 20.

Subdivisions into one, two, three and four sub-domains were created by merging these basic sub-domains. The dimensions of the specimen and the parameters of incident laser beam were the same as in the previous case.

The results show that larger number of sub-domains leads to higher accuracy, which confirms the findings already reported in the past [9–11].

The temperature change in time at two different locations on the upper surface of the mono-layer specimens, for the same type of problem as above, in the cases of constant as well as linearly temperature-dependent absorption coefficient, with $A_0 = 0.642$ and $B = -4.28 \times 10^{-4}\,1/\mathrm{K}$ (Eq. (3)) are shown in Fig. 9. A domain decomposition with four sub-domains and ATPS-RBF was used, with the same nodes' arrangement as in the

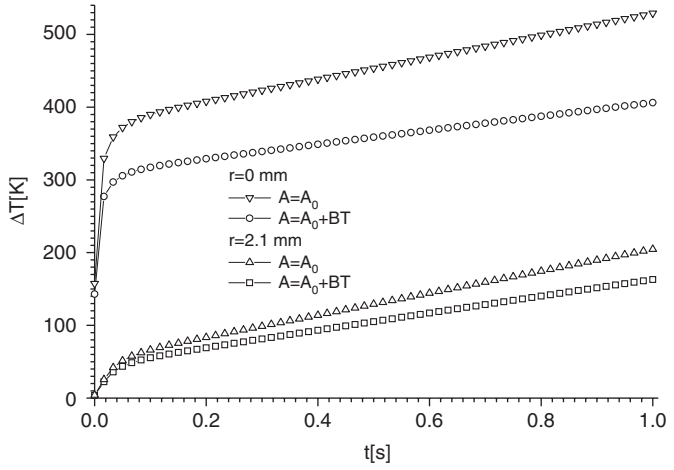

Fig. 9. Change of temperature in time on the upper surface at two different locations on the mono-layer specimen for cases of constant and linear temperature dependence of the absorption coefficient.

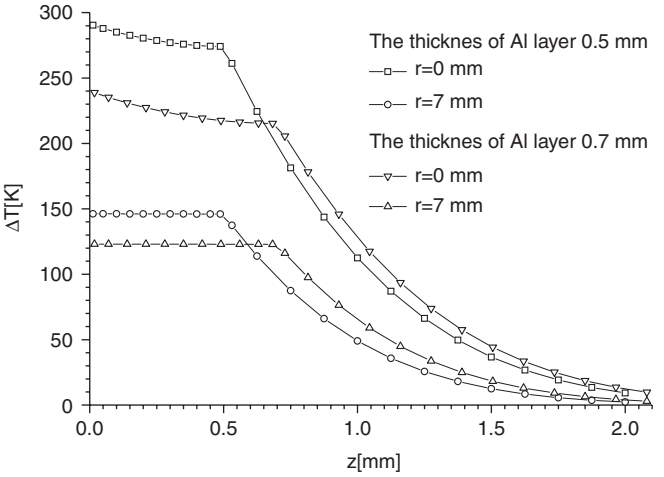

Fig. 10. The distributions of the temperature differences in axial direction in case of two layer structures (Al–Glass) for two thicknesses of Al layer, obtained by the DRM-MD with nine sub-domains for two values of coordinate r.

examples presented in Figs. 3 and 4. The dimensions of the specimen and the parameters of the incident laser beam were the same as in the previous case. The results show that the case of constant absorption coefficient leads to higher temperatures on the specimen's surface.

5.2. Case study 2

The geometry of the problem considered is shown in Fig. 1. The upper layer of the two-layer structure is made of Al and the lower layer is made of glass. The following dimensions of the structures were used: (i) Al-layer—0.5 mm, glass layer—4.5 mm; and (ii) Al-layer—0.7 mm, glass layer—4.3 mm thicknesses. In both cases the radius of the specimen was 7 mm. The following properties of the laser beam were assumed: power—100 W, radius of laser beam—1 mm, the laser beam has constant intensity with the top head profile and time duration of 1 s. The following coefficients were used for the glass layer: $\lambda_g = 0.582\,\mathrm{W/m\,K}$; $c_g = 770\,\mathrm{J/kg}$; $\rho_g = 2400\,\mathrm{kg/m^3}$; $a_g = \rho/\lambda c$ and $\alpha_g = 0.02425\,\mathrm{W/m^2\,K}$.

Fig. 10 shows the distributions of temperature field in axial direction at $r = 0$ and 7 mm. The results show that as the Al layer is thicker, the temperature achieved is lower because of the high thermal conductivity of Al.

Because of non-homogeneity and large difference between the physical parameters of materials (glass and Al), for small time steps the numerical procedure may become unstable, which was found out to be the case for the ATPS RBF. When this function was used the results got less accurate and only time steps larger than 0.052 s could be used. For smaller time steps the numerical procedure became unstable. In this case MQ-RBFs with shape parameter $c = 10^{-4}$ were used leading to satisfactory accuracy and stability of the solution. A domain decomposition with nine sub domains, rectangular in shape, and 1181 nodes (504-boundary nodes and 677-interior ones) was used. A linear temperature dependence of the absorption coefficient was assumed (Eq. (3)).

5.3. Case study 3

The next example has been solved by Wrobel et al. [16] using BEM approach based on fundamental solution including elliptic integrals. The geometry and boundary conditions in cases of solid and hollow cylinders are presented in Figs. 11(a) and (b), respectively. Because of the symmetry only one half of the hollow cylinder was discretized.

Domain decomposition with nine sub-domains was used with a total number of 953 nodes in the case of the solid cylinder (504-boundary nodes and 449-internal nodes) and 729 in the case of hollow one (376-boundary nodes and 353-internal nodes).

In Tables 1 and 2 the numerical results obtained by Wrobel et al. [16] and the present DRM-MD approach with ATPS-RBFs are shown, for the case of the steady-state temperature distribution inside solid and hollow cylinders, respectively. The numerical results are compared to analytical solution. It can be observed that the DRM-MD approach with the present formulation achieved accuracy of the same order as the approach applied by Wrobel et al. [16]. This indicates that the present formulation represents a useful alternative for solving axisymmetric problems taking into account the simplicity of implementation for the present formulation compared to the formulation based on fundamental solution for axisymmetric problems.

6. Conclusion

A DRM-MD approach for axisymmetric heat transfer problems was developed for the case of material heating with laser radiation.

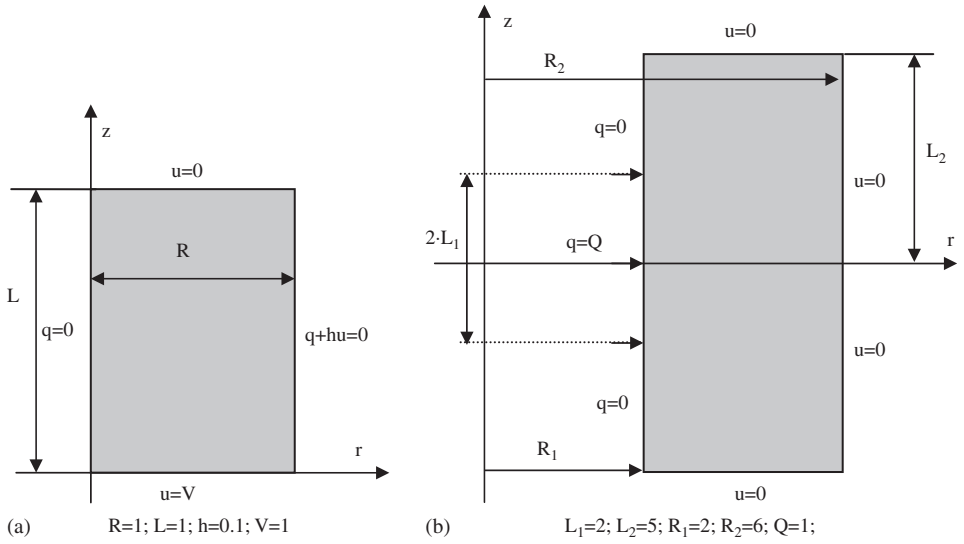

Fig. 11. The geometry, boundary conditions and numerical values for all parameters, in case of solid and hollow cylinder [17].

Table 1
The numerical results for the temperature distribution on the outside boundary ($R = 1$) of the solid cylinder using DRM-MD approach (9 sub-domains, ATPS-RBFs) for axisymmetric geometry, compared to BEM and the analytical solutions [17]

z	BEM (constant)	BEM (linear)	Analytical	DRM-MD
0.375	0.807	—	0.805	0.8051
0.500	—	0.751	0.751	0.7510
0.875	0.606	—	0.604	0.6043
1.000	—	0.560	0.560	—
1.375	0.437	—	0.436	0.4357
1.500	—	0.397	0.397	0.3972
1.875	0.289	—	0.289	0.2887
2.000	—	0.254	0.254	—
2.375	0.155	—	0.156	0.1559
2.500	—	0.124	0.124	0.1242

Table 2
The numerical results for the temperature distribution inside the hollow cylinder using DRM-MD approach (9 sub-domains, ATPS-RBFs) for axisymmetric geometry, compared to BEM and analytical solutions [17]

r	z	BEM (constant)	BEM (linear)	Analytical	DRM-9MD
3.0	4.0	0.140	0.141	0.141	0.1406
3.0	3.0	0.317	0.320	0.319	0.3183
3.0	2.0	0.556	0.556	0.556	0.5571
3.0	1.0	0.762	0.760	0.761	0.7626
3.0	0.0	0.832	0.831	0.831	0.8322
5.0	4.0	0.043	0.043	0.043	0.0431
5.0	3.0	0.088	0.088	0.088	0.0884
5.0	2.0	0.133	0.133	0.133	0.1329
5.0	1.0	0.167	0.167	0.167	0.1669
5.0	0.0	0.180	0.180	0.180	0.1796

The thermal model of laser–material interaction in cases of mono layer as well as multi-layer structures was considered. This approach was used for solving the time-dependant governing equation with corresponding boundary and initial conditions for the axisymmetric case. The time derivative was approximated by finite difference.

The spatial distributions of temperature fields inside the multi-layer structures were analyzed. The effect of

temperature dependence of the absorption coefficient on the process of laser heating was taken into account.

The accuracy of the developed DRM-MD approach was tested on three case studies including: mono and two-layer structures for transient case and absorption coefficient which is either constant or linearly dependent on temperature, as well as steady-state temperature distribution inside solid and hollow cylinders. The numerical results were compared towards analytical solutions as well as numerical results obtained using fundamental solution for axysimmetric case (based on elliptic integrals). Different number of sub-domains and different RBFs were considered, leading to good accuracy and showing high flexibility and easy in implementation.

The developed approach can be used in the case of multi-layer structures and non-linear or non-homogenous problems [23].

References

[1] Wood RM. Laser damage in optical materials. Bristol and Boston: Adam Hilger; 1986.
[2] Khuri-Leal S, Hurza GJ. Aesthetic laser surgery. J Geriatr Dermatol 1995;3:249–64.
[3] Gagliano FP, Lumley RH, Watkins LS. Laser in Industry. Proc IEEE 1969;57(2):114–47.
[4] Rykalin N, Uglov A, Kokora A. Laser machining and welding. Moscow: Mir Publishers; 1979. p. 57–68.
[5] Bojanic S. Analyzing of laser-material interaction with condensed matter at viewpoint of physical models. PhD thesis, University of Belgrade, 1997.
[6] Nardini D, Brebbia CA. A new approach to free vibration analysis using boundary elements. Appl Math Model 1983;7:157–62.
[7] Brebbia CA, Tells JC, Worbel LC. Boundary element techniques. Berlin, Heidelberg, New York, Tokyo: Springer; 1984.
[8] Ramdas Ram-Mohan L. Finite element and boundary element applications in quantum mechanics. Oxford University Press; 2002.
[9] Popov V, Power H. A domain decomposition in the dual reciprocity approach. Bound Elem Commun 1996;7/1:1–5.
[10] Popov V, Power H. DRM-MD approach for the numerical solution of gas flow in porous media, with applications to landfill. Eng Anal Bound Elem 1999;23:175–88.
[11] Popov V, Power H. The DRM-MD integral equation method: an efficient approach for the numerical solution of domain dominant problems. Int J Numer Methods Eng 1999;44:327–53.
[12] Florez W, Power H, Chejne F. Multi-domain dual reciprocity BEM approach for the Navier–Stokes system of equations. Commun Numer Methods Eng 2000;16:671–81.
[13] Florez W, Power H, Janna FC. Multi-domain dual reciprocity for the solution of inetastic non-Newtonian flow problems at low Reynolds number. Comput Mech 2001;27(5):396–411.
[14] Samardzioska T, Popov V. Numerical comparison of the equivalent continuum, non-homogeneous and dual porosity models for flow and transport in fractured porous media. Adv Water Resour 2005;28: 235–55.
[15] Peratta A, Popov V. A new scheme for numerical modelling of flow and transport processes in 3D fractured porous media. Adv Water Resour 2006;29:42–61.
[16] Wrobel LC, Telles JCF, Brebbia CA. A dual reciprocity boundary element formulation for axisymmetric diffusion problems. In: Brebbia CA, editor. Boundary elements VIII. Boston: Computational Mechanics Publications; 1986. p. 59–69.
[17] Wang K, Mattheij RMM, ter Morsche HG. Alternative DRM formulations. Eng Anal Bound Elem 2003;27:175–81.
[18] Bai Fengwu, Lu Wen-Qiang. The selection and assemblage of approximation functions and disposal of its singularity in axisymmetric DRBEM for heat transfer problems. Eng Anal Bound Elem 2004;28:955–65.
[19] Patridge PW, Brebbia CA, Wrobel L. The dual reciprocity boundary element method. London & New York: Computational Mechanics Publication, Southampton and Elsevier Applied Science; 1992.
[20] Buhmann MD. Radial basis functions: theory and implementations. Cambridge University Press; 2003.
[21] Natalini B, Popov V. An alternative approach for calculation of the first and higher order derivatives in the DRM-MD. Eng Anal Bound Elem 2004;28:61–78.
[22] Gospavic R, Sreckovic M, Popov V. Modelling of laser-material interaction using semi-analytical approach. Math Comput Simul 2004;65:211–9.
[23] Sutradhar A, Paulino G, Grar LJ. Transient heath conduction in homogeneous and non-homogeneous materials by the Laplace transform Galerkin boundary element method. Eng Anal Bound Elem 2002;26:119–32.
[24] Natalini B, Popov V. Tests of radial basis functions in the 3D DRM-MD. Commun Numer Methods Eng 2006;22:13–22.